Ultrafast Dynamics of Solute-Solvent Complexation Observed at Thermal Equilibrium in Real Time

Junrong Zheng, Kyungwon Kwak, John Asbury,* Xin Chen, Ivan R. Piletic, M. D. Fayer†

In general, the formation and dissociation of solute-solvent complexes have been too rapid to measure without disturbing the thermal equilibrium. We were able to do so with the use of two-dimensional infrared vibrational echo spectroscopy, an ultrafast vibrational analog of two-dimensional nuclear magnetic resonance spectroscopy. The equilibrium dynamics of phenol complexation to benzene in a benzene–carbon tetrachloride solvent mixture were measured in real time by the appearance of off-diagonal peaks in the two-dimensional vibrational echo spectrum of the phenol hydroxyl stretch. The dissociation time constant τ_d for the phenol-benzene complex was 8 picoseconds. Adding two electron-donating methyl groups to the benzene nearly tripled the value of τ_d and stabilized the complex, whereas bromobenzene, with an electron-withdrawing bromo group, formed a slightly weaker complex with a slightly lower τ_d. The spectroscopic method holds promise for studying a wide variety of other fast chemical exchange processes.

Solvents play an enormous role in practical chemistry by influencing the reactivity of dissolved substrates (*1*). In part, the influence stems from polarization effects or nonspecific solute-solvent interactions for which the solvent structure around a solute can be described in terms of an isotropic radial distribution function (*2*). However, specific intermolecular interactions, such as hydrogen bonding, can lead to structurally characterizable solute-solvent complexes that are constantly forming and dissociating under thermal equilibrium conditions on very short time scales (*3*). The dynamics of these transient species can play an important role in the physical and chemical properties of a solute-solvent system by affecting reaction rates, reaction mechanisms, and product ratios (*1*).

If the complexes persist for microseconds or longer, their thermal equilibrium dissociation and exchange dynamics can be studied by means of two-dimensional (2D) nuclear magnetic resonance (NMR) techniques (*4*–*6*). However, for the majority of organic and other types of nonaqueous solutions, in which a vast number of reactions take place, the solute-solvent complexes are bound by energies on the order of a few k_BT (where k_B is the Boltzmann constant and T is absolute temperature; $k_BT \approx 0.6$ kcal/mol at room temperature) and therefore form and dissociate on subnanosecond time scales. As a result, NMR studies cannot distinguish the rapid exchange events and can offer only a dynamically averaged view of the system.

Ultrashort laser pulses have long offered a means of probing rapid dynamics. However, ultrafast absorption and fluorescence techniques have been hindered by the need to perturb the chemical properties of the system in order to study it. These techniques measure net changes in state populations. Thus, electronic excitation can be used to initiate a reaction on a femtosecond time scale by placing a molecule in a higher electronic state, with subsequent fast probing of new product formation, but the system is then no longer observed in its chemical equilibrium state. What is needed to probe equilibrium solvent-solute interactions is an ultrashort analog of 2D NMR spectroscopy. Here, we apply such an analog—ultrafast 2D infrared (2D IR) vibrational echo spectroscopy—to probe the dynamics of phenol complexation with several benzene-based solvents.

Coherent spectroscopy: From NMR to IR. Both the NMR and IR vibrational echo techniques involve pulse sequences that induce and then probe the coherent evolution of excitations (nuclear spins for NMR and vibrations for IR) of a molecular system. The molecules in a given environment (for example, free versus complexed) are induced to "oscillate" in spin states or vibrational states, all at the same time and with the same phase by the first pulse in the sequence. The effect of the first pulse, along with the manipulation of the phase relationships among the vibrational oscillators by the following pulses in the sequence, is an important feature that 2D IR vibrational echo spectroscopy has in common with 2D NMR. The later pulses generate observable signals that are sensitive to change in environments of individual molecules during the experiment (e.g., from free to complexed solute or vice versa), even if there is no change of aggregate populations in the distinct environments (the observable in linear spectroscopy). The critical difference between the IR and NMR variants is that the IR pulse sequence acts on a time scale six orders of magnitude faster than the NMR sequence.

Vibrational echo–based 2D IR experiments have been applied to the study of the intramolecular coupling of vibrational modes (v), the structure of proteins, and the dynamics of hydrogen bonds by observing the positions of peaks or the change in the shape of peaks in the 2D spectrum (*7*–*9*). In the present study, intermolecular chemical exchange causes new peaks in the spectrum to appear and grow, yielding the rate of chemical exchange.

Phenol binds weakly to benzene. Intermolecular chemical exchange under thermal equilibrium conditions is ubiquitous in nature. It forms the basis for supramolecular chemistry (*10*), host-guest chemistry (*10*), chemical and biological recognition (*11*), and self-assembly (*10*). The dynamics of complexes involving noncovalent interactions with aromatic rings are pivotal to the protein-ligand recognition and concomitantly to drug design (*11*). The phenol-benzene complex cuts to the essence of interactions between protic and hydrophobic groups so widespread in proteins and surfactants. More fundamentally, the specific attraction between the polar OH group on phenol and the polarizable π-electron cloud on benzene is an intriguing intermediate case between dispersion forces and hydrogen bonding. The phenol-benzene complex appears to be mainly a van der Waals interaction (*12*), although it is also referred to as π-hydrogen bonding (*11*, *13*) and has recently been found to be of biological importance. π-Hydrogen bonding can stabilize α helices in proteins and plays an important role in cellular and synaptic signal transmission (*13*).

The formation enthalpy for the gas-phase phenol-benzene complex is ~4 kcal/mol (*12*). The gas-phase structure has been determined by electronic structure calculations (*14*). Figure 1 shows two views of the structure of the phenol-benzene complex. In contrast to chemical intuition, the hydroxyl group does not point to the center of the benzene ring, but rather points between adjacent carbons. One of the ortho hydrogens on the phenol also points

Department of Chemistry, Stanford University, Stanford, CA 94305, USA.

*Present address: Department of Chemistry, Pennsylvania State University, University Park, PA 16802, USA.

†To whom correspondence should be addressed. E-mail: fayer@stanford.edu

between a pair of carbons that are on the opposite side of the benzene ring. Additional higher level electronic structure calculations performed as part of this study confirm this structure and show that the other complexes studied here have similar structures. Previous studies in liquids demonstrate the existence of the phenol-benzene complex and have measured its enthalpy of formation in CCl_4 (1.56 kcal/mol at room temperature) in temperature-dependent linear IR absorption experiments (*15*) (see below).

We used 2D IR vibrational echo spectroscopy to extract the binding kinetics of phenol-benzene complexes in solution. In addition, we have examined the effect of modifying benzene with electron-donating groups (*p*-xylene or *p*-dimethylbenzene) and an electron-withdrawing group (bromobenzene). Experimental specifics are described below for the benzene studies, with results from the corresponding substituted benzene studies given at the end for comparison.

For the purposes of our experimental study, phenol presents several advantages. The hydroxyl stretch is an isolated vibration with a strong absorption cross section and relatively long vibrational lifetime, so IR excitation is efficient and there is a sufficient time window to observe its dynamics. Moreover, the hydroxyl stretch frequency is sensitive to formation of the complex with benzene. By deuterating the hydroxyl group (OD rather than OH), we transferred the stretching mode away from aromatic C-H stretching bands of similar frequency. The OD stretching band of free phenol in pure CCl_4 is centered at 2665 cm^{-1} (Fig. 2, dotted curve). The spectrum of phenol in pure benzene shows a red-shifted (lower energy) band in this region at 2631 cm^{-1} (Fig. 2, dashed curve), resulting from formation of the phenol-benzene complex. By diluting the benzene with CCl_4, we can shift the equilibrium toward more free phenol. At the concentrations used here in the mixed solution (phenol/benzene/CCl_4 molar ratio 2:40:100, respectively), the absorptions of free and complexed phenol are both prominent in the spectrum (Fig. 2, solid line). Integration of these bands, calibrated from the pure samples, yields the concentrations of complexed and free phenol, which in turn determine the equilibrium constant for complex formation (K_{eq} = [complex]/[phenol][benzene] = 0.26 at 298 K).

To measure the formation and dissociation kinetics of the complex in this solution, we apply three successive IR pulses with the same polarization, which induce the subsequent emission in a distinct direction of a time-delayed fourth pulse—the vibrational echo. The transform-limited pulses (50 fs, <4 cycles of light) are produced using a Ti:sapphire regeneratively amplified laser system coupled to an optical parametric oscillator, and they span sufficient bandwidth (300 cm^{-1} centered at ~4 μm, or 2500 cm^{-1}) to cover the $v = 0$ to $v = 1$ (hereafter denoted 0-1) and 1-2 transitions of the hydroxyl OD stretching modes in both free and complexed phenol. The echo pulse is detected, with frequency and phase resolution, by combining with a fifth (local oscillator) pulse, and the combined pulse is dispersed in a spectrograph. Data are thus obtained as a function of three variables: the emitted echo frequency ω_m (measured directly by the spectrograph), the variable time delay between the first and second pulses (τ), and the variable time delay between the second and third pulses (T_w, the variable "waiting" time). By numerical Fourier transform (FT), the τ scan data taken at each T_w are mapped to a second frequency variable ω_τ. The data are then plotted in three dimensions, showing the amplitude as a function of both ω_τ and ω_m (which correspond to the ω_1 and ω_3 axes, respectively, in 2D NMR). The experimental setup is shown in fig. S1; further experimental details are given in (*16*).

Chemical exchange creates new off-diagonal peaks. Figure 3 displays the 2D IR vibrational echo spectra as contour plots at a very short T_w (200 fs, Fig. 3A) and a long T_w (14 ps, Fig. 3B) (1 fs = 10^{-3} ps = 10^{-15} s). The data have been normalized to the largest peak at each T_w. The red contours are positive-going (0-1 vibrational transition) and the blue contours are negative-going (1-2 vibrational transition). As discussed below, the 0-1 signal comes from two quantum pathways that are related to bleaching of the ground state and stimulated emission, both of which produce a vibrational echo pulse that is in phase with (and therefore adds to) the local oscillator pulse to produce a positive-going signal. The 1-2 signal arises because there is a new absorption that was not present before the first two excitation pulses. The 1-2 vibrational echo pulse is 180° out of phase with (and thus subtracts from) the local oscillator to produce

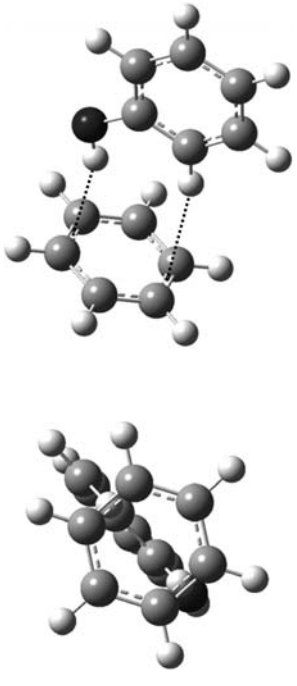

Fig. 1. Two views of the structure of the phenol-benzene complex calculated with DFT at B3LYP/6-31+ G (d,p) level in the gas phase.

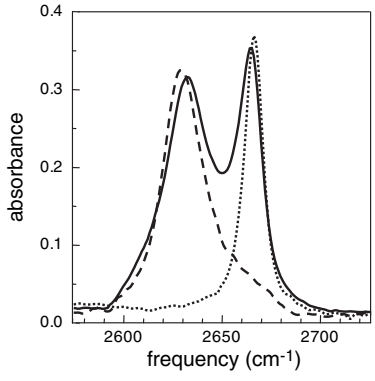

Fig. 2. FT-IR absorption spectra of the OD stretch of phenol-OD (hydroxyl H replaced with D) in CCl_4 (free phenol, dotted curve), phenol in benzene (benzene-phenol complex, dashed curve), and phenol in the mixed benzene-CCl_4 solvent (2:5 molar ratio), which displays absorptions of both free and complexed phenol (solid curve).

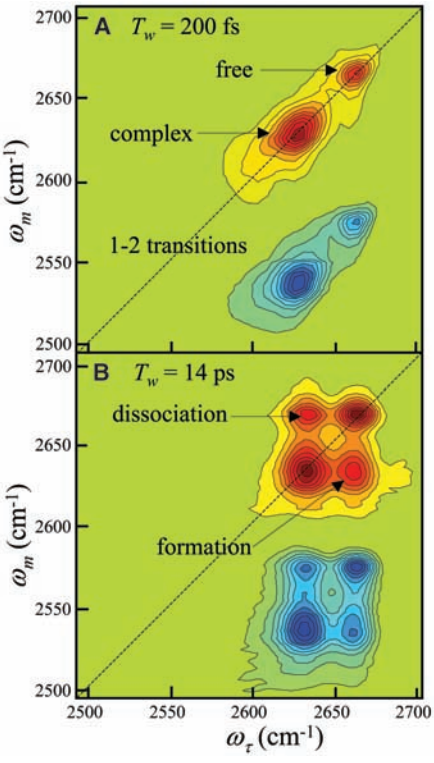

Fig. 3. 2D IR vibrational echo spectra of the OD stretch of phenol in the mixed benzene-CCl_4 solvent. Each contour represents a 10% change. (**A**) Data for T_w = 200 fs. The red contours on the diagonal (positive going) are the 0-1 transitions of the free phenol and the phenol-benzene complex. The blue contours off the diagonal (negative going) are the corresponding 1-2 transition peaks. (**B**) Data for T_w = 14 ps. Additional peaks have grown in because of chemical exchange, that is, the formation and dissociation of the phenol-benzene complex.

a negative-going signal. At T_w = 200 fs, there are two peaks on the diagonal (0-1 transitions) and the corresponding 1-2 transition peaks are off-diagonal. There are no off-diagonal peaks in the 0-1 region because 200 fs is short relative to the exchange time; by contrast, T_w = 14 ps (Fig. 3B) is long relative to the exchange time, and additional peaks have grown in.

The 2D IR vibrational echo spectra in Fig. 3, A and B, can be understood in terms of time-dependent diagrammatic perturbation theory, which describes the nonlinear optical interactions with the molecular vibrations (*17*, *18*). (See fig. S2 for detailed diagrams showing how all the peaks are generated.) The frequency at which the first pulse excites a mode is the mode frequency on the ω_τ axis (horizontal axis): 2631 cm^{-1} for the 0-1 transition in free phenol and 2665 cm^{-1} for the complex. The third pulse induces the vibrational echo pulse, which is emitted after a time delay at the precise frequency of the vibrational transition that interacted with that third pulse. The frequency of the vibrational echo emission is the frequency on the ω_m axis (the vertical axis). In Fig. 3A, the data are taken before chemical exchange. For the 0-1 vibrational transitions, the third pulse induces the vibrational echo emission at the same frequencies excited by the first pulse, so there are two peaks on the diagonal where $\omega_\tau = \omega_m$ (red peaks in Fig. 3A). If the frequency of vibrational echo emission (ω_m, third pulse frequency) is different from the frequency of initial excitation (ω_τ, first pulse frequency), peaks will appear off-diagonal. Again, in Fig. 3A, the blue peaks are off-diagonal by the vibrational anharmonicity (*19*) because the modes are initially excited at their 0-1 frequencies (ω_τ) but the third pulse causes vibrational echo emission at their 1-2 frequencies (ω_m). Even in the absence of chemical exchange, the peaks observed at very short T_w delays (Fig. 3A) will undergo evolution with increasing T_w, because of both spectral diffusion (*17*, *18*, *20*) (see below), which changes the shapes of the peaks, and vibrational lifetime decay and orientational relaxation, which cause the peaks to decay in amplitude.

The influence of chemical exchange on the 2D correlation spectrum can be easily understood in terms of the ideas presented above. If some complexed phenols are liberated during the T_w period, then the third pulse will cause the emission of the vibrational echo at the frequency of the free phenol OD stretch. The frequency of emission ω_m then differs from the excitation frequency ω_τ for these specific molecules. The result will be an off-diagonal peak that appears only if chemical exchange occurs. Because the free phenol absorbs at higher frequency than complexed phenol, this off-diagonal peak is shifted to higher frequency along the ω_m axis by the frequency difference (34 cm^{-1}) between the free and complexed modes. Conversely, if some free phenols bind to benzene during the T_w period, then the third pulse will produce an off-diagonal peak for these (formerly) free phenols, which is shifted to lower frequency along the ω_m axis by the same amount. Identical considerations apply for both the 0-1 and 1-2 regions of the spectrum. This behavior is shown in Fig. 3B, wherein substantial chemical exchange has led to the generation of a block of four red peaks and a block of four blue peaks; the two new peaks in each block were not present at T_w = 200 fs. Clearly some complexes have dissociated and others have formed. The growth of the additional off-diagonal peaks with increasing T_w is directly related to the time dependence of the chemical exchange.

The phenol-benzene complex persists for 8 ps. Figure 4 displays the time evolution of the correlation spectrum in the 0-1 transition region as 3D representations. (More plots are shown in fig. S3.) The data have been normalized to the largest peak at each T_w. As in Fig. 3, at T_w = 200 fs there are only diagonal peaks. The peak in the foreground is the vibration echo of complexed phenol. At T_w = 2 ps, two changes are evident. First, the shapes of the diagonal peaks have altered. Whereas at T_w = 200 fs the peaks are elongated along the diagonal, by 2 ps they have become symmetrically rounded. The change in shape is caused by spectral diffusion. At short times, the vibrational transitions are inhomogeneously broadened. As time proceeds, the fluctuations in the solvent environment cause the transition frequency to sample all possible values, and each line becomes dynamically broadened. The change in shape provides information on the dynamic solute-solvent interactions, but here we focus our analysis exclusively on the chemical exchange. At 2 ps, the off-diagonal peaks are just becoming visible. By 5 ps, the off-diagonal peaks are clearly evident, and they continue to grow in amplitude, as shown in the 10-ps and 14-ps plots.

Simple inspection of the data reveals that the phenol-benzene complexes form and dissociate on a picosecond time scale. To obtain quantitative rates, we fit the data with the use of time-dependent diagrammatic perturbation theory and kinetic equations to describe the exchange dynamics. Because of spectral diffusion, the shapes of the peaks change. In the absence of all other dynamical processes, the change in shape preserves the volume of a peak, but the peak amplitude is reduced as the peak broadens along the ω_τ axis. Therefore, the integrated peak volumes are fit to obtain the population dynamics. There are three processes that contribute to the change in the peak volumes: the OD vibrational lifetime relaxation in free and complexed phenol (lifetimes T_1^f and T_1^c), the orientational relaxation (time constants τ_r^f and τ_r^c), and the chemical exchange (dissociation and formation rate constants k_d and k_f). The kinetic scheme is shown in Fig. 5A; more details are described in fig. S4. The vibrational relaxation and orientational relaxation lead to diminishing intensities of all peaks with increasing time. Even complete orientational randomization during the T_w period does not cause the vibrational echo to decay to zero. Therefore, the chemical exchange time need not be short relative to the orientational relaxation time. The chemical exchange causes the diagonal peaks to diminish and the off-diagonal peaks to grow, as can be seen in Figs. 3 and 4. The dissociation rate (number per unit time) of the complex equals the formation rate if the system is in equilibrium (see below). The complex dissociation time constant τ_d is independent of concentration and is therefore used here ($\tau_d = 1/k_d$, where k_d is the dissociation rate constant; the dissociation rate is k_d[complex]).

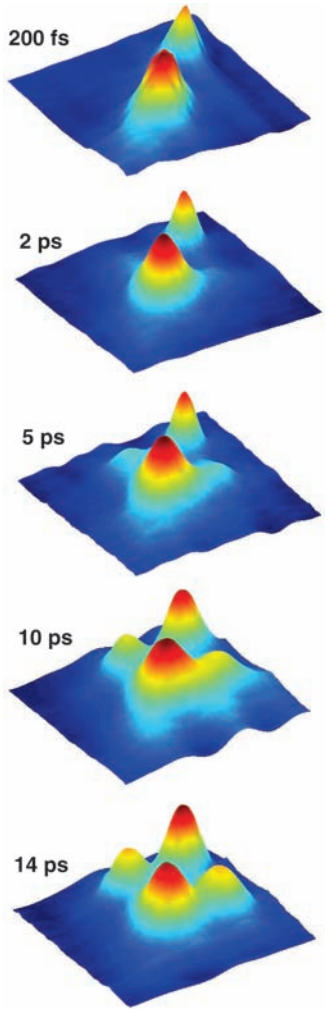

Fig. 4. The time dependence of the 2D IR vibrational echo spectrum in the 0-1 transition region. As T_w increases, the off-diagonal peaks grow in because of chemical exchange (formation and dissociation of the benzene-phenol complex). Between 200 fs and 2 ps, the peaks change shape because of spectral diffusion. Inspection of the data shows a picosecond time scale for the chemical exchange (growth of the off-diagonal peaks).

The data for the 0-1 transition region consist of four time-dependent components: the two diagonal peaks (complexed and free phenol) and the two off-diagonal peaks (dissociation and formation of complexes during the experiment). A similar treatment is applied for the 1-2 region below. All four peaks can be reproduced with the single fitting parameter τ_d. The input parameters used are $T_1^c = 10$ ps, $T_1^f = 12.5$ ps, $\tau_r^c = 3.4$ ps, $\tau_r^f = 2.9$ ps, and the ratio of the complexed and free phenol concentrations [complex]/[free] = 0.8. The lifetimes and the orientational relaxation times were measured with polarization-selective IR pump-probe experiments (*21*) on the OD stretch of the complex in pure benzene solvent and free phenol in pure CCl_4 solvent. The orientational relaxation time constants were corrected for the small viscosity difference between the pure solvents and mixed solvents. The concentration ratio was measured with linear absorption FT-IR spectroscopy.

Figure 5B shows the peak volume data for the 0-1 transition region of the spectrum as a function of T_w. The fits (solid curves) to the time dependence of all of the peaks using a single adjustable parameter, τ_d, are very good. From the fits, dissociation of the complex proceeds with a time constant $\tau_d = 8 \pm 2$ ps. The error bars obtained from the single-parameter fits are smaller than 2 ps. The cited error bars mainly arise from the uncertainties in all of the parameters in the calculation, rather than the quality of the fit.

Vibrational excitation does not perturb the equilibrium. An important aspect of 2D NMR is that the manipulation of spin states by a pulse sequence produces a negligible perturbation of the molecular system, and therefore the experiment does not move the system away from equilibrium. It is possible to determine whether vibrational excitation in the current system shifts the concentrations away from their equilibrium values or changes τ_d. Even if vibrational excitation does shift the system out of equilibrium, the dynamics for the equilibrium system can nonetheless be extracted. If the thermal equilibrium is not perturbed by vibrational excitation, both off-diagonal peaks (formation and dissociation of the complex) should have the same time dependence. In the 0-1 transition region, the integrated off-diagonal intensities (circles and squares in Fig. 5B) do show matching growth rates as a function of T_w, confirming an undisturbed equilibrium. In other words, the pulse sequence has no impact on the aggregate populations of free and bound phenol in solution. For each complex formed during the T_w period, another complex liberates a phenol.

It is possible that vibrational excitation changes both the dissociation rate and the complex formation rate. If both rates were changed to the same extent, the equilibrium concentrations would be unchanged and the off-diagonal peaks would grow in at the same rate, as observed. It is possible to test whether vibrational excitation changes the dissociation time constant τ_d directly and conclusively. Of more importance, it is possible to see how the equilibrium exchange time constants can be extracted even if vibrational excitation does change the dynamics of dissociation and formation of complexes.

A series of qualitative energy level/kinetic diagrams (Fig. 6) clarifies how to do this and enables a more detailed understanding of the 2D vibrational echo measurements of chemical exchange. These diagrams are not rigorous quantum mechanical diagrams as used in diagrammatic perturbation theory, but their simplicity has important heuristic value. (The full set of double-sided Feynman diagrams pertaining to this problem is given in fig. S2.) The diagrams show how the off-diagonal peaks for the dissociation of complexed phenol to free phenol ($c \rightarrow f$) are generated in both the 0-1 (Fig. 6, A and B) and the 1-2 (Fig. 6C) portions of the 2D spectrum. These are the peaks at $\omega_\tau = 2631$ cm^{-1} and $\omega_m = 2665$ cm^{-1} (0-1), and at $\omega_\tau = 2631$ cm^{-1} and $\omega_m = 2575$ cm^{-1} (1-2) in Fig. 3B. The other off-diagonal peaks, representing complex formation, arise in the same manner.

The signal for the off-diagonal 0-1 portion $c \rightarrow f$ peak has two contributions illustrated in Fig. 6, A and B. In Fig. 6A, the arrow representing pulse 1 makes a coherent superposition state of the $v = 0$ and $v = 1$ levels of the phenol-benzene complexes at frequency

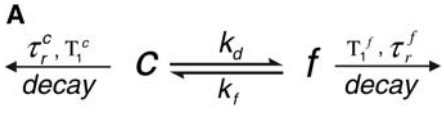

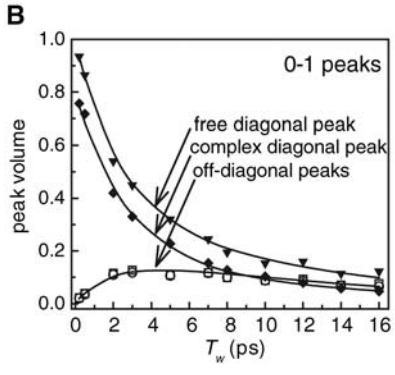

Fig. 5. (**A**) Kinetic scheme. The complexed (c) and free (f) phenols can exchange with dissociation rate constant k_d and formation rate constant k_f. The exchange process causes the off-diagonal peaks to grow in and the diagonal peaks to diminish. All of the peaks decay because of vibrational relaxation with lifetime T_1^i and rotational relaxation with time constant τ_r^i. (**B**) Peak volume data (scaled with extinction coefficient differences; see fig. S4) and fits to the data. There is one adjustable parameter to fit all of the data: the dissociation time constant, τ_d, of the phenol-benzene complex. Fits to the data for the four peaks in the 0-1 transition region give $\tau_d = 8$ ps. The two off-diagonal peaks (circles and squares) grow in at the same rate, showing that the thermal equilibrium is not perturbed by vibrational excitation to the first vibrationally excited state of the hydroxyl stretch.

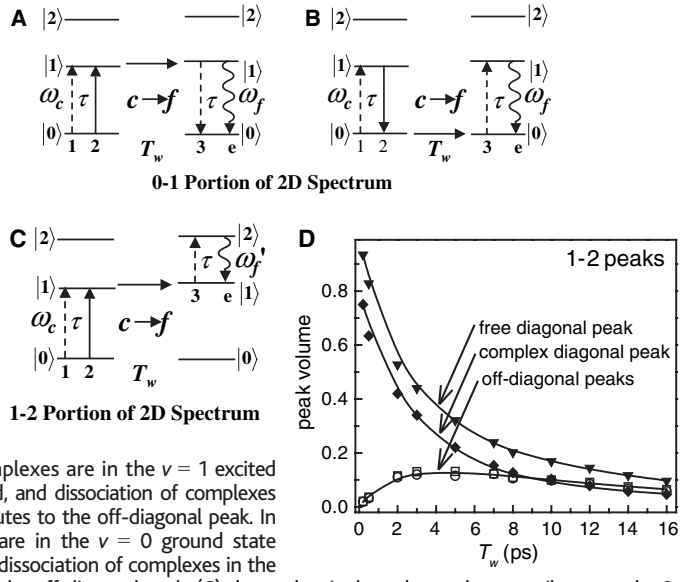

Fig. 6. (**A** to **C**) Energy level/kinetic diagrams that show the pulse sequence pathways that give rise to the vibrational echo signal for the off-diagonal peaks created by the dissociation of the phenol benzene complex in the 0-1 and 1-2 portions of the 2D vibrational echo spectrum (Fig. 3B). (A) and (B) show the two pathways for the 0-1 portion of the spectrum. Each pathway contributes half of the 0-1 dissociation off-diagonal peak. In pathway (A), complexes are in the $v = 1$ excited state during the T_w period, and dissociation of complexes in the $v = 1$ state contributes to the off-diagonal peak. In pathway (B), complexes are in the $v = 0$ ground state during the T_w period, and dissociation of complexes in the $v = 0$ state contributes to the off-diagonal peak. (C) shows the single pathway that contributes to the 0-1 dissociation off-diagonal peak in the 1-2 portion of the spectrum. In pathway (C), complexes are in the $v = 1$ excited state during the T_w period. Only complexes that dissociate while in the excited state contribute to the dissociation off-diagonal peak in the 1-2 portion of the spectrum. The difference between the two contributions to the signal for the 0-1 portion and the single contribution for the 1-2 portion permit the extraction of the equilibrium dissociation time even if vibrational excitation changes the dissociation and formation rate constants from their equilibrium values (see text). (**D**) Data and calculated curves for the 1-2 portion of the spectrum (blue peaks in Fig. 3B) give the same τ_d value as the 0-1 portion, demonstrating that excitation of the hydroxyl stretch does not influence the dissociation rate constant.

ω_c. In all diagrams, a dashed arrow represents the creation of a coherent superposition state. A coherent superposition state is equivalent to an in-plane precessing magnetization that is generated by the first pulse in a 2D NMR pulse sequence. During the τ period between pulses 1 and 2, exchange does not contribute to the growth of the off-diagonal peak, because the exchange time τ_d is long relative to the inverse of the frequency difference between the *c* and *f* peaks. Therefore, jumps from *c* to *f* will produce an ensemble of superposition states in *f* with random phase, resulting in no contribution to the off-diagonal peak signal. After time τ, the second pulse generates a population in the excited $v = 1$ state. A solid arrow in all diagrams represents the generation of a population. Some of the molecules that are initially complexes have now been "labeled" in the $v = 1$ state. If some of these complexes dissociate ($c \rightarrow f$) during the period T_w, pulse 3 will produce a coherent superposition state (dashed arrow in Fig. 6A) oscillating at frequency ω_f. The vibrational echo pulse will be emitted (wavy arrow) at frequency ω_f. Therefore, the ω_τ frequency is ω_c, but the ω_m frequency is ω_f. The $c \rightarrow f$ off-diagonal peak is produced. The pathway in Fig. 6A for which the dissociation occurs with molecules labeled in $v = 1$ accounts for half of the $c \rightarrow f$ off-diagonal peak signal in the 0-1 portion of the spectrum.

The pathway shown in Fig. 6B accounts for the other half of the $c \rightarrow f$ off-diagonal peak signal. Again, pulse 1 produces a 0-1 coherent superposition state (dashed arrow), but pulse 2 produces a population (solid arrow) in the $v = 0$ state instead of in the $v = 1$ state, again labeling molecules that are initially complexes. This pathway involves molecules labeled in the $v = 0$ state during the T_w period. For those complexes that undergo dissociation during the T_w period, pulse 3 will produce a coherent superposition state (dashed arrow) at frequency ω_f, and the vibrational echo (wavy arrow) will be emitted at ω_f. As in the path shown in Fig. 6A, in Fig. 6B the ω_τ frequency is ω_c, but the ω_m frequency is ω_f, and this path contributes to the $c \rightarrow f$ off-diagonal peak. For both pathways, pulse 3 produces a coherent superposition state. In NMR, this coherent superposition state yields an in-plane precessing magnetization (a macroscopic oscillating magnetic dipole moment) that is detected with a pickup coil. In the vibrational experiment, the coherent superposition state in each pathway gives rise to a macroscopic oscillating electric dipole moment that emits light, the vibrational echo pulse (wavy arrows).

The important point to see from Fig. 6, A and B, is that half of the signal comes from molecules that are in their $v = 1$ state during the T_w period and half comes from molecules in the $v = 0$ state. If vibrational excitation influences the equilibrium dynamics, then the time evolution of the exchange off-diagonal peaks will be affected and τ_d can be altered from its equilibrium value. Whether τ_d is changed by vibrational excitation can be tested; if it is, then its equilibrium value can be recovered by examining the 1-2 portion of the 2D vibrational echo spectrum in addition to the 0-1 portion. Figure 6C shows the single diagram that contributes to the $c \rightarrow f$ off-diagonal peak in the 1-2 portion of the spectrum. In Fig. 6C, pulse 1 creates a 0-1 coherent superposition state (dashed arrow) and pulse 2 generates a population (solid arrow) of complexed phenols in the $v = 1$ state. There is only one path because it is necessary to have molecules in the $v = 1$ state so that pulse 3 can produce a coherent superposition state (dashed arrow) of $v = 1$ and $v = 2$, which is then followed by vibrational echo emission at the 1-2 frequency (blue peaks in Fig. 3B). If dissociation of complexed phenols occurs during the T_w period, the blue $c \rightarrow f$ off-diagonal peak is generated. Thus, the entire signal for this off-diagonal peak arises solely from complexes that were in the $v = 1$ state and underwent dissociation during the T_w period.

This property does not hold for the red $c \rightarrow f$ off-diagonal peak, for which half of the signal is generated by molecules that were in the $v = 1$ state and half by molecules in the $v = 0$ state during the T_w period. If excitation to the vibrationally excited $v = 1$ state changes the equilibrium dynamics, then the τ_d determined from the 0-1 portion of the spectrum will be different from the τ_d determined from the 1-2 portion of the spectrum. The τ_d value determined from the 0-1 portion of the spectrum is an average of its ground state and first vibrationally excited state value. Using the two values of τ_d determined from the 0-1 and 1-2 portions of the 2D vibrational echo spectrum, the value for the ground state (unperturbed thermal equilibrium) pathway can be easily obtained. If the two values are the same, then vibrational excitation did not have an experimentally measurable influence on the equilibrium dynamics of the system.

Figure 6D shows the data and calculated curves for the 1-2 region of the 2D vibrational echo spectrum. There are no adjustable parameters. The data are reproduced with the identical parameters used for the 0-1 region, including $\tau_d = 8$ ps. Variation of τ_d does not improve the agreement. Thus, within experimental uncertainty, for the phenol-benzene complex and the other systems studied here, exciting the hydroxyl stretch has no influence on the dissociation time and, as discussed above, vibrational excitation does not change the equilibrium constant.

Electron-rich benzene derivatives make stronger complexes. In addition to the phenol-benzene complex, the phenol-bromobenzene and phenol–*p*-xylene complexes were studied in the identical manner. The dissociation time for the phenol–*p*-xylene complex is considerably slower than for the phenol-benzene complex, with $\tau_d = 21 \pm 3$ ps. The dissociation time constant for the phenol-bromobenzene complex is $\tau_d = 6 \pm 3$ ps. This value is within experimental uncertainty of the phenol-benzene complex τ_d. However, the error bars are determined in large part by the errors of all of the parameters used in the calculations, rather than by the quality of the fits. A direct comparison for the phenol-benzene and phenol-bromobenzene complexes (at, for example, 7 ps) of the sizes of their diagonal peaks versus their respective dissociation-induced off-diagonal peaks clearly shows that the bromobenzene complex dissociates more rapidly.

To investigate the trend in the τ_d values, we measured the temperature dependences of the complexation equilibria for all three systems by IR absorption and then used these values to determine the bond enthalpies, ΔH^0, of the complexes. (Here, the standard solvent concentrations are defined to be the concentrations used in the experiments.) The ΔH^0 values extracted from van't Hoff plots were –1.21 kcal/mol for the phenol-bromobenzene complex, –1.67 kcal/mol for the phenol-benzene complex, and –2.23 kcal/mol for the phenol–*p*-xylene complex (fig. S5). Thus, as the bond enthalpy increases (stronger bond), the dissociation time also increases. If the free energy of activation for dissociation ($\Delta G^\ddagger$) scales with the bond enthalpies, we can qualitatively understand the trend in τ_d. The electron-withdrawing bromine weakens the complex by reducing the π-electron density of the ring, leading to a faster dissociation time. Conversely, in *p*-xylene, the electron-donating methyl groups increase the π-electron density of the ring, resulting in a stronger complex and correspondingly longer dissociation time.

The 2D IR vibrational echo technique is general. The method used here is general for measuring fast chemical exchange dynamics in the ground electronic state, and appears promising for studies of a wide range of molecular isomerizations and electron and proton transfer processes under thermal equilibrium conditions. There are three conditions necessary to apply this technique to study thermal equilibrium exchange phenomena: (i) There must be at least one IR active mode that has a distinct frequency for each species undergoing exchange, (ii) the concentrations of all the equilibrated species must be high enough for detection, and (iii) the exchange rate must be comparable to or shorter than the vibrational lifetime of the vibration that is being used as the probe. It is important to note that the vibrational mode that is used as the probe need not be directly involved in the exchange process, as is the hydroxyl stretch used in this study. It is sufficient that the exchange causes the mode frequency to change.

References and Notes

1. C. Reichardt, *Solvents and Solvent Effects in Organic Chemistry* (Wiley-VCH, Weinheim, Germany, ed. 3, 2003).
2. G. J. Throop, R. J. Bearman, *J. Chem. Phys.* **42**, 2408 (1965).
3. S. N. Vinogradov, R. H. Linnell, *Hydrogen Bonding* (Van Nostrand Reinhold, New York, 1971).
4. J. Jeener, B. H. Meier, P. Bachmann, R. R. Ernst, *J. Chem. Phys.* **71**, 4546 (1979).
5. B. H. Meier, R. R. Ernst, *J. Am. Chem. Soc.* **101**, 6441 (1979).
6. A. G. Palmer, *Chem. Rev.* **104**, 3623 (2004).
7. N. Demirdoven, M. Khalil, O. Golonzka, A. Tokmakoff, *J. Phys. Chem. A* **105**, 8030 (2001).
8. Y. Kim, R. M. Hochstrasser, *J. Phys. Chem. B* **109**, 6884 (2005).
9. J. B. Asbury *et al.*, *Phys. Rev. Lett.* **91**, 237402 (2003).
10. H.-J. Schneider, A. K. Yatsimirsky, *Principles and Methods in Supramolecular Chemistry* (Wiley, Chichester, UK, 2000).
11. E. A. Meyer, R. K. Castellano, F. Diederich, *Angew. Chem. Int. Ed. Engl.* **42**, 1210 (2003).
12. J. L. Knee, L. R. Khundkar, A. H. Zewail, *J. Chem. Phys.* **87**, 115 (1987).
13. M. F. Perutz, *Philos. Trans. R. Soc. London Ser. A* **345**, 105 (1993).
14. A. Fujii, T. Ebata, N. Mikami, *J. Phys. Chem. A* **106**, 8554 (2002).
15. G. C. Pimentel, A. L. McClellan, *Annu. Rev. Phys. Chem.* **22**, 347 (1971).
16. J. B. Asbury, T. Steinel, M. D. Fayer, *J. Lumin.* **107**, 271 (2004).
17. S. Mukamel, *Annu. Rev. Phys. Chem.* **51**, 691 (2000).
18. S. Mukamel, *Principles of Nonlinear Optical Spectroscopy* (Oxford Univ. Press, New York, 1995).
19. O. Golonzka, M. Khalil, N. Demirdoven, A. Tokmakoff, *Phys. Rev. Lett.* **86**, 2154 (2001).
20. J. B. Asbury *et al.*, *J. Chem. Phys.* **121**, 12431 (2004).
21. H.-S. Tan, I. R. Piletic, M. D. Fayer, *J. Chem. Phys.* **122**, 174501(9) (2005).

22. We thank J. I. Brauman for insightful discussions, J. Xie for his aid in chemical preparation, and H.-S. Tan for his aid in pump-probe measurements. Supported by grants from the Air Force Office of Scientific Research (F49620-01-1-0018) and NSF Division of Materials Research (DMR-0332692).

Supporting Online Material

www.sciencemag.org/cgi/content/full/1116213/DC1
Materials and Methods
Figs. S1 to S5

16 June 2005; accepted 26 July 2005
Published online 4 August 2005;
10.1126/science.1116213
Include this information when citing this paper.